Core-Gap-Shell Nanoparticles@Polyaniline with Tunable Plasmonic Chiroptical Activities by pH and Electric Potential Dual-Modulation

Han Lin [a], *Hideyuki Mitomo** [b], *Yusuke Yonamine* [b], *Zhiyong Guo** [c], *Kuniharu Ijiro** [b]

a. Graduate School of Life Science, Hokkaido University, Kita 10, Nishi 8, Kita-Ku, Sapporo 060-0810, Japan

b. Research Institute for Electronic Science, Hokkaido University, Kita 21, Nishi 10, Kita-Ku, Sapporo 001-0021, Japan

c. State Key Laboratory for Managing Biotic and Chemical Threats to the Quality and Safety of Agro-products, School of Material Science and Chemical Engineering, Ningbo University, Ningbo 315211, P. R. China

ABSTRACT: The emerging concept of tunable plasmonic chirality is mostly observed as a reconfigurable behavior or a feature of complex chiral plasmonic assemblies. For discrete colloidal particles, it is challenging to achieve reversible tunability or a transient response with regard to chiroptical activities, particularly in the visible or near-infrared region. Herein, we demonstrate a stimulus-responsive system based on chiral molecule-achiral plasmonic nanoparticles coated with polyaniline (PANI) as the variable dielectric layer, in which L/D-cysteine molecules are introduced between the gold core and the shell as a static chiral source, allowing the chiral transfer effect to be greatly amplified by the hot spot gap of sub-monomolecular thickness. By taking advantage of the responsive properties to either pH or the electric potential dual stimuli of PANI, which also provides a stable and real-time switchable dielectric environment for the whole system, dynamic tuning of the plasmon and its induced chiroptical activities of core-gap-shell nanoparticles@PANI were precisely obtained. This well-defined design provides an open platform for flexible and rational tailoring of plasmonic cores, chiral molecules, and variable dielectrics to chiroptical needs, which is important for realizing applications in chemical sensing, chiral nanocatalysis, enantioselective separations, and novel optical devices.

Introduction

Chirality refers to the geometric structure of an object that cannot be superimposed on its mirror image by translation or in-plane rotation.[1] Optically, substances with chiral characteristics also exhibit differences in the absorption of left- or right-handed circularly polarized (LCP or RCP) light, known as circular dichroism (CD).[2] Notably, the CD responses of most chiral biomolecules are generally located in the ultraviolet (UV) region and show extremely weak activity, often

requiring high concentrations to support them.[3] Recent studies have demonstrated an interesting form of coupling between chiral molecules and metal nanoparticles, which is associated with the localized surface plasmon resonance (LSPR) phenomenon, the strong electromagnetic field of which is able to enhance the CD signals of surface chiral molecules.[4-9] Meanwhile, chiral molecules can also induce dissipative chiral currents arising inside the particles and provide the feedback of a new CD response near the LSPR position of the particles. This effect is termed plasmon-induced chirality, CD_{LSPR} or $CD_{plasmon\text{-}induced}$.[10-12]

In principle, the chirality of a substance is a static and well-defined property.[13] However, CD_{LSPR}, a novel optical response that is active in the visible and near-infrared regions, depending on the molecular conformation as well as the LSPR properties of the nanoparticles, has attracted great interest in the field of chiral plasmonics with regard to the customization and dynamic tuning of chiroptical activities, such as signal intensity changes or response reversals, as well as wavelength shifts.[7] To date, most studies on reconfigurable active chiral plasmonic nanostructures have focused on dimeric or three-dimensional (3D) assemblies.[14-18] For example, the artificial tuning or inversion of CD responses was achieved by the appropriate modulation of the chiral templates (e.g., DNA origami, cellulose liquid crystals, etc.) or manipulation of the behavior of nanoparticle assembly/disassembly with the assistance of external stimuli.[19-27] However, there have been very few reports on the dynamically tunable plasmonic chiroptical activities of discrete metal nanoparticles, especially in wavelength shifts, mainly due to the vulnerability of most chiral molecules to external stimuli as well as the instability of the nanoparticles and their unadjustable LSPR wavelength (λ_{LSPR}).[28, 29]

Except for assembly/disassembly strategies, it is generally difficult to actively and reversibly tune the λ_{LSPR} of plasmonic nanoparticles with a specific composition, shape and size.[30] The λ_{LSPR} of simple spherical or rod-shaped particles is as follows:[28]

$$\lambda_{LSPR} = \lambda_P(2\varepsilon_m + 1)^{-1/2}$$

where λ_P is the wavelength corresponding to the plasma frequency and ε_m is the environment dielectric constant to influence the LSPR peak position of the particle. Obviously, the variable dielectric material makes discrete active plasmonics possible. PANI, as an easily fabricated and inexpensive variable dielectric material, has received a good deal of attention due to its excellent stability, fascinating redox chemistry and doping/de-doping properties.[31] Recently, its stability in water has been greatly improved by doping with anionic surfactants, which has led to many studies on the tunable plasmonic properties of PANI with gold nanocrystals.[32-36] Interestingly, based on the mechanism of plasmon-induced chirality generation, it makes reasonable to achieve tunable chiral shifting activities with the assistance of the tunable λ_{LSPR}. However, there are no reports to date on the use of dielectric active layers such as PANI to generate discrete plasmon-induced tunable chiral activities, especially with dual modulation.

Herein, we demonstrate an active plasmonic chiroptical system based on chiral core-gap-shell gold nanoparticles@PANI (c-CGS Au NPs@PANI). The gold nanorod (Au NR) used as a core was loaded with cysteine (Cys) molecules as a chiral source, forming a gap of sub-monolayer thickness by the regrowth of the Au shell. This gap structure with a natural electromagnetic field hot spot significantly enhanced the CD_{LSPR} response. At the same time, the inert Au shell acted as a protective layer to prevent external stimuli from disturbing the Cys molecules. Finally, the active dielectric layer PANI was coated on the Au shell surface to provide a reconfigurable dielectric

environment for the whole system (c-CGS Au NRs@PANI, Scheme 1), leading to the tunable LSPR and resulting in CD_{LSPR} optical activities within the visible region in response to the external pH and electric potential modulation. Satisfyingly, c-CGS Au NRs@PANI exhibited a wider wavelength range of CD_{LSPR} modulation (around 60 nm shift), stability (more than 100 cycles), accuracy (10 nm/V), and fast switching response (< 1 s), further enhancing their potential in fields such as chiral optical device fabrication.

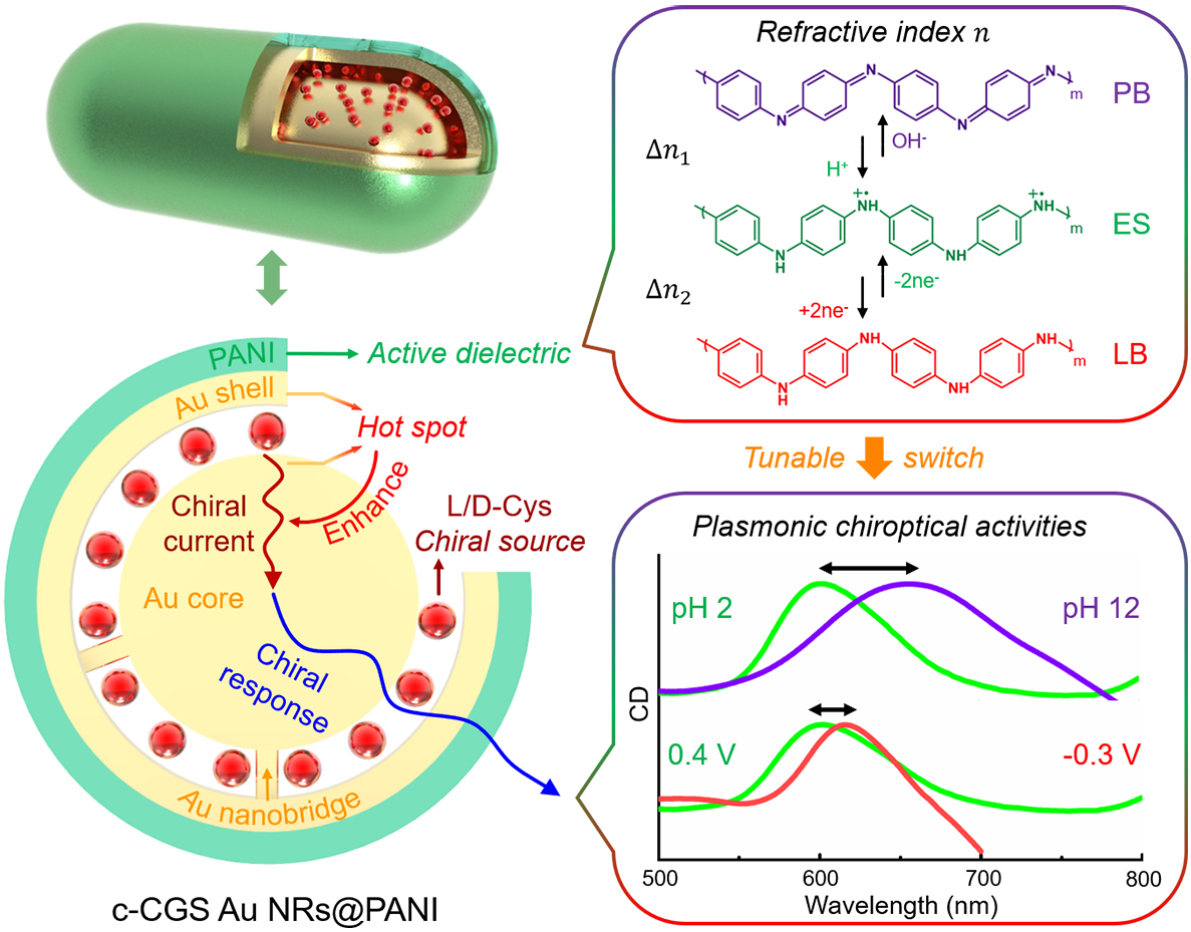

Scheme 1. The c-CGS Au NRs@PANI-based dual-modulable active plasmonic chiroptical system.

Results and Discussion

Growth mechanism, morphology and chiral response of c-CGS Au NRs. The c-CGS Au NRs were prepared by the regrowth of Au NRs as cores (Figure 1 and S1), on which different concentrations of L/D-Cys were adsorbed as a chiral source (Figure S2), providing a gap of sub-monomolecular thickness between the Au core and the shell. The Cys molecules induce superimposed oscillations of the electrons within the core in the transverse or longitudinal axis, generating dissipative chiral currents and thereby providing feedback to the chiral response.[37] Therefore, in this mode, the position of the emerging CD band was near the plasmon resonance band of the metal nanoparticles (Figure 1J). In addition, Cys, as molecules that can form a strong bond with the Au surface, reduce the surface energy of the core, and the regrowth mainly followed the Volmer–Weber mode (island growth); i.e., the growth mainly proceeded from the "Au nanobridges" with relatively high surface energy sites (Figure S3).[38, 39] Finally, the shell was formed by connecting the adjacent nanobridges and defining the intragap with the core. Although the intragap may be discontinuous and so little spacing could be observed on TEM images (Figure S4), the extinction spectral shifts on T- and L-LSPR to longer wavelength could support the gap formation (Figure 1J, S1). Importantly, these c-CGS Au NRs showed greatly enhanced chiral responses compared to the case before shell growth (Figure S5), and the intensity was almost unchanged after removal of the Cys molecules from the outer surface of the shell (Figure S6), suggesting that the enhancement effect arose from the natural electromagnetic field hot spots at the intragap. This has also been substantiated by the simulations of the proposed effective medium theory, which employed a similar model of chiral molecules being encapsulated in a nanocavity, with the origin of the chiral response attributed to the electromagnetic near field enhancement.[40, 41] The intensity and position of the chiral peak were more dependent on the molecular density, the

number of hot spots, and the geometry of the plasmonics.[42-44] During shell growth, the low concentration (5 nM) of Cys molecules was unable to support a significant chiral response, due to the less quantity of chiral sources and hot spots (Figure 1A-C, J top), while medium concentration (50 nM) was considered to have the opportunity to increase both of chiral sources and hot spot density while maintaining the simple rod shape (Figure 1D-F). Further increasing the concentration (500 nM), a large number of free strong ligands bonding immediately to freshly exposed crystal faces induced locally anisotropic growth and inhibited the formation of hot spots. The high-density chiral molecules on the crystal faces may also direct the enantioselective deposition of Au atoms, resulting in a distinct chiral morphological character (Figure 1G-I).[13, 45] This was not an ideal situation for the tailoring and manipulation of the LSPR properties and CD responses, as these rely heavily on the morphology of the particles and would become more complicated under the above conditions (Figure 1J bottom, S7). It was found that the LSPR characteristics were related to the Cys concentration, but not to the conformation. In contrast, opposite chiral responses were obtained for L- and D-Cys, depending on the orientation of the electric dipole of the molecule with respect to the vector $\vec{R}$ of particle, i.e., the exciton-plasmon interactions model.[4] Moreover, different from Au NPs, the observation of $CD_{T\text{-}LSPR}$ and $CD_{L\text{-}LSPR}$ in opposite directions induced by homochiral Cys molecules. It could also be explained by this model, since the respective interactions dominated by the same electric dipole with the transverse or longitudinal axis vectors of Au NRs, were also perpendicular to each other.[46, 47]

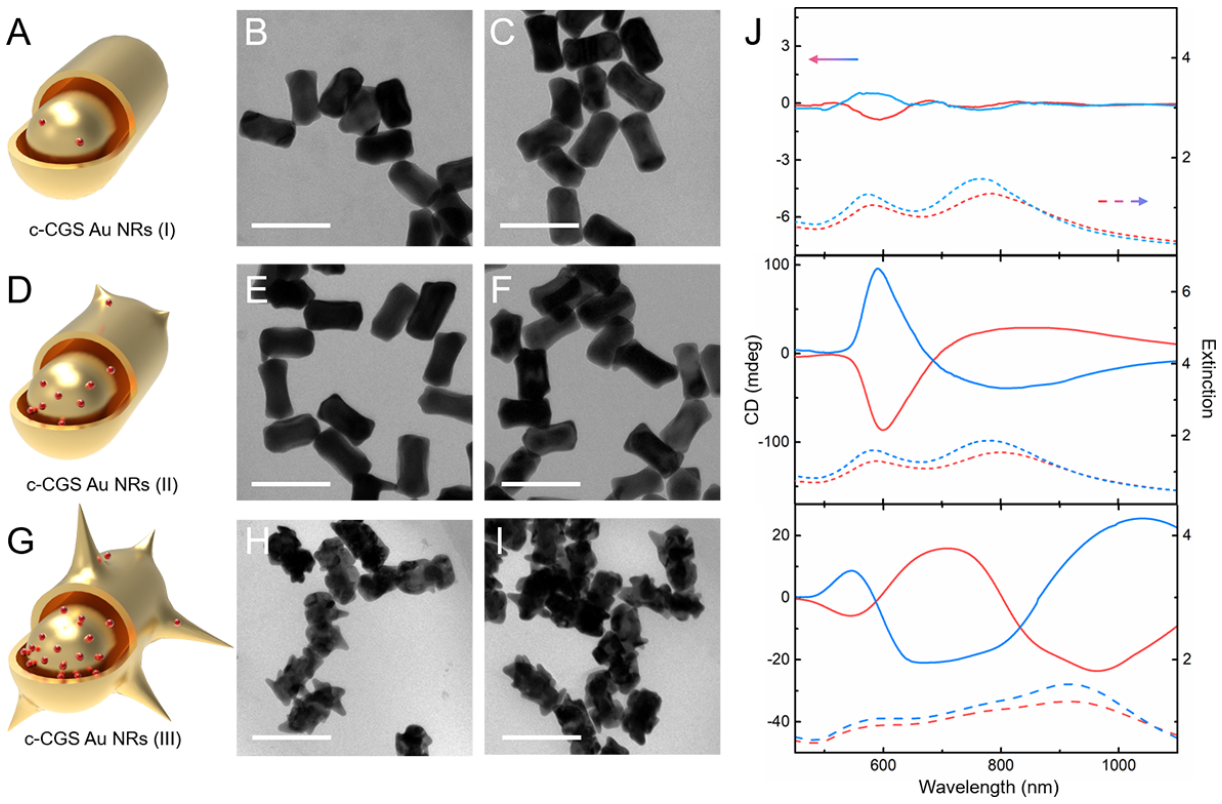

133

134 **Figure 1.** Characteristics of c-CGS Au NRs. (A) Schematic illustration of c-CGS Au NRs (I)
135 prepared using 5 nM of Cys with TEM images (L-Cys: (B), D-Cys: (C)). (D) Schematic illustration
136 of c-CGS Au NRs (II) prepared using 50 nM of Cys with TEM images (L-Cys: (E), D-Cys: (F)).
137 (G) Schematic illustration of c-CGS Au NRs (III) prepared using 500 nM of Cys, with TEM
138 images (L-Cys: (H), D-Cys: (I)). (J) CD (solid curves) and extinction (dashed curves) spectra of
139 c-CGS Au NRs synthesized in the presence of different concentrations of Cys (top 5 nM; middle
140 50 nM, and bottom 500 nM). Red and blue curves correspond to L-Cys and D-Cys groups,
141 respectively. The scale bars are 200 nm. CD spectra at 800-900 nm were recovered by fitting a
142 Bessel curve in origin software due to the severe disturbance by the light source conversion. The
143 raw spectra were shown in the supporting (Figure S8).

Interestingly, although it is an indisputable fact that the L-LSPR of Au NRs possesses a more prominent advantage in the active plasmonics, the stronger chiral response is a necessary prerequisite to be considered for active chiral plasmonics.[48, 49] As shown in Figure 1J middle and S9, $CD_{T\text{-}LSPR}$ of c-CGS Au NRs (II) showed the strongest chiral intensity, with a *g*-factor about 0.0015 in absolute value around 600 nm, implying nonnegligible potential in active chiral plasmon studies. Furthermore, in consideration of the fact that the LSPR of Au nanospheres (Au NSs) is close to the T-LSPR of Au NRs in terms of extinction spectrum, similar c-CGS Au NSs were prepared (Figure S10). Although the c-CGS Au NSs also exhibited an enhancement for the chiral signal compared to the Cys-attached Au NSs, their CD intensity was still very weak and was accompanied by strong background noise (Figure S11). The reason for this may be their isotropic structure, which provides less potential for symmetry breaking of the internal electron oscillation paths, resulting in lower resonance coefficients, poorer chiral activities, and weaker tunability.[4, 50]

Optimisation of PANI dielectric layer thickness. Next, to tune the position of the LSPR and CD_{LSPR}, PANI coating was performed by surfactant-assisted chemical oxidative polymerization.[32] Correspondingly, the LSPR shifts of plasmonic nanoparticles follow the relationship shown below:[28]

$$\Delta\lambda_{shift} = m\Delta n\left(1 - e^{-2d/l_d}\right)$$

where m is the refractive index sensitivity of the plasmonic nanoparticle, Δn is the variation of refractive index between different dielectric environments, d is the effective thickness of the dielectric environment, and l_d is the decay length of the electromagnetic field on the plasmonic nanoparticle surface. Obviously, the maximum $\Delta\lambda_{shift}$ is strongly related to the Δn and d values. It is well known that PANI can exist in six states with different refractive indices at various

pH values and redox states: leucoemeraldine base (LB), leucoemeraldine salt (LS), emeraldine base (EB), emeraldine salt (ES), pernigraniline base (PB), and pernigraniline salt (PS).[51] The conditions or means to accomplish the full state transformation are often severe, such as strong acidic environments, changes in aqueous and non-aqueous electrolyte environments and higher potentials, which will directly affect the lifetime of the materials. In contrast, ES (n_{ES} ≈1.40), PB (n_{PB} ≈2.05), LB (n_{LB} ≈1.68) can be transformed in a relatively gentle manner.[34] It should be noted that the PANI layer thickness was important in terms of the following two points. The first point is the need to maximise the shift qualities of the LSPR peaks ($\Delta\lambda_{shift}$) as well as the potential CD_{LSPR} peak wavelength. The second point is the need to avoid excessive loss of chiral response. As shown in Figure S12A, B, the *g*-factor of the asymmetry parameter for c-CGS Au NRs (II) decreased after coating. This may be due to the achiral PANI shells increasing the total absorption, but having little effect on the absorption of LCP or RCP light. Additionally, a very low specific value for the *g*-factor was observed for the composite structure with the Au NSs as the core (Figure S12C, D), also indicating that anisotropic nanostructures are more suitable for active chiral plasmons. Based on the above considerations, the ideal situation is to obtain a larger peak shift by application of a thinner PANI layer, while avoiding the possible loss of CD signal intensity in response to external stimuli.

We obtained the L-Cys induced c-CGS Au NRs (II)@PANI (L-c-CGS Au NRs (II)@PANI) with a layer thickness of 7 nm, 11 nm or 14 nm by repeating the polymerization cycles (Figure 2A-D). As the PANI forming the outermost layer existed in the ES state, its refractive index was slightly larger than that of water ($n_{H_2O} \approx$ 1.33), resulting in a gradual red-shift of the T-LSPR positions after coating (Figure 2E, S13). To understand their LSPR characteristics, the L-c-CGS Au NRs (II)@PANI and pure PANI solutions were observed at both pH 2 and pH 12 (Figure 2F,

S14). At pH 2, the T-LSPR (590 nm) and longitudinal LSPR (L-LSPR, 797 nm) could be easily distinguished, and the ES state itself presented an extinction peak at 875 nm. At pH 12, the ES state was converted into the PB state (556 nm) due to the de-doping of protons, and the proximity of PB and T-LSPR led them to be coupled into a broad peak (646 nm). The red-shift of the L-LSPR (from 797 to 863 nm) was also evidenced by the change from the ES to the PB state. For reference, similar LSPR shifts occurred in the case of c-CGS Au NSs@PANI (Figure S15A, B). As shown in Figure S16, the $\Delta\lambda_{shift}$ of the composite structure with a PANI layer of 11 nm and 14 nm were the same. Considering the overall chiral loss due to the PANI layer, we chose c-CGS Au NRs (II) coated with an 11-nm thick PANI layer for the following studies.

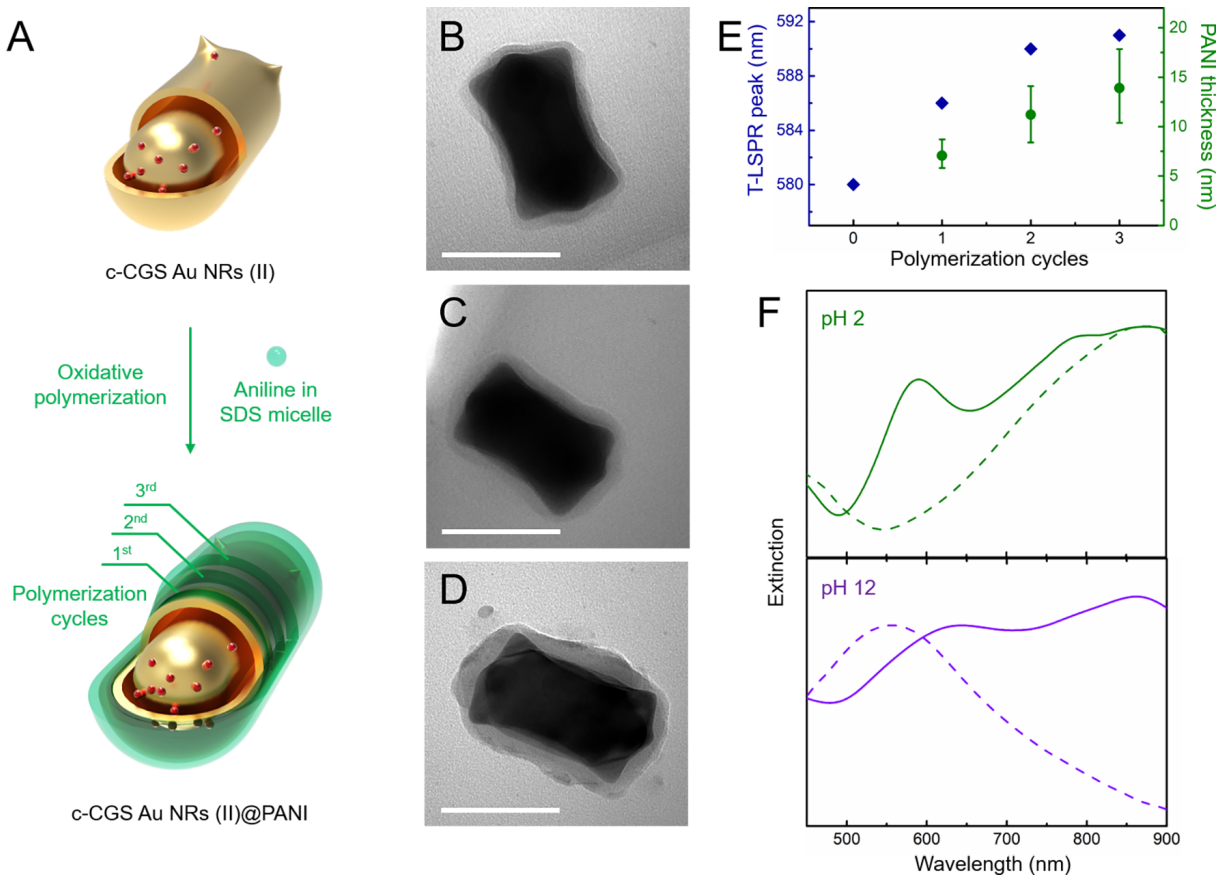

Figure 2. Characteristics of c-CGS Au NRs (II)@PANI. (A) Schematic illustration for coating c-CGS AuNRs (II) with a PANI layer. TEM images of L-c-CGS Au NRs (II)@PANI after (B) one, (C) two, (D) three polymerization cycles. (E) T-LSPR peak positions at pH 2 and PANI layer thickness versus the number of polymerization cycles. (F) Normalized extinction spectra of L-c-CGS Au NRs (II) coated with an 11-nm thick PANI layer (solid curves) and pure PANI (dashed curves) in the ES (green) and PB (purple) states. The scale bars are 100 nm.

pH-Responsive plasmonic and plasmon-induced chiral activities. Our exploration of the mechanism of pH modulation in more detail (Figure 3A) revealed the L-c-CGS Au NRs (II)@PANI aqueous solution displayed a visual transition from coffee to eggplant violet at pH 2 and pH 12, respectively (Figure 3B). Then, using L-c-CGS Au NRs (II)@PANI as a typical case (Figure 3C), the T-LSPR peak at 590 nm was not disturbed by the ES peak at a pH of 2, and the corresponding $CD_{T\text{-}LSPR}$ peak was also located nearby (601 nm), both of which had narrow peak widths. As shown in Figure 3D, after the H^+ in the solution was completely consumed by OH^-, the H^+ in the outer layer of the PANI "microenvironment" participated in the neutralization, with de-doping leading to the start of the transition to the PB state, which explains the sudden change in peak positions starting around pH 8. The change in peak positions was not significant between pH 10 and 12, indicating that the PANI had completed proton de-doping. Ultimately, the T-LSPR peak red-shift was about 57 nm to 647 nm, while the corresponding $CD_{T\text{-}LSPR}$ peak also completed a similar red-shift (Figure 3F-H, S17A-C). Such a significant chiral peak shift cannot be explained solely by the contribution of changes in dielectric constant and the T-LSPR itself, which suffered from the low sensitivity of T-LSPR, but also on the contribution of the PB state involved in the peak coupling.[52] Similar results were observed in the case of D-c-CGS Au NRs (II)@PANI (Figure 3E, I-K and S17D-F).

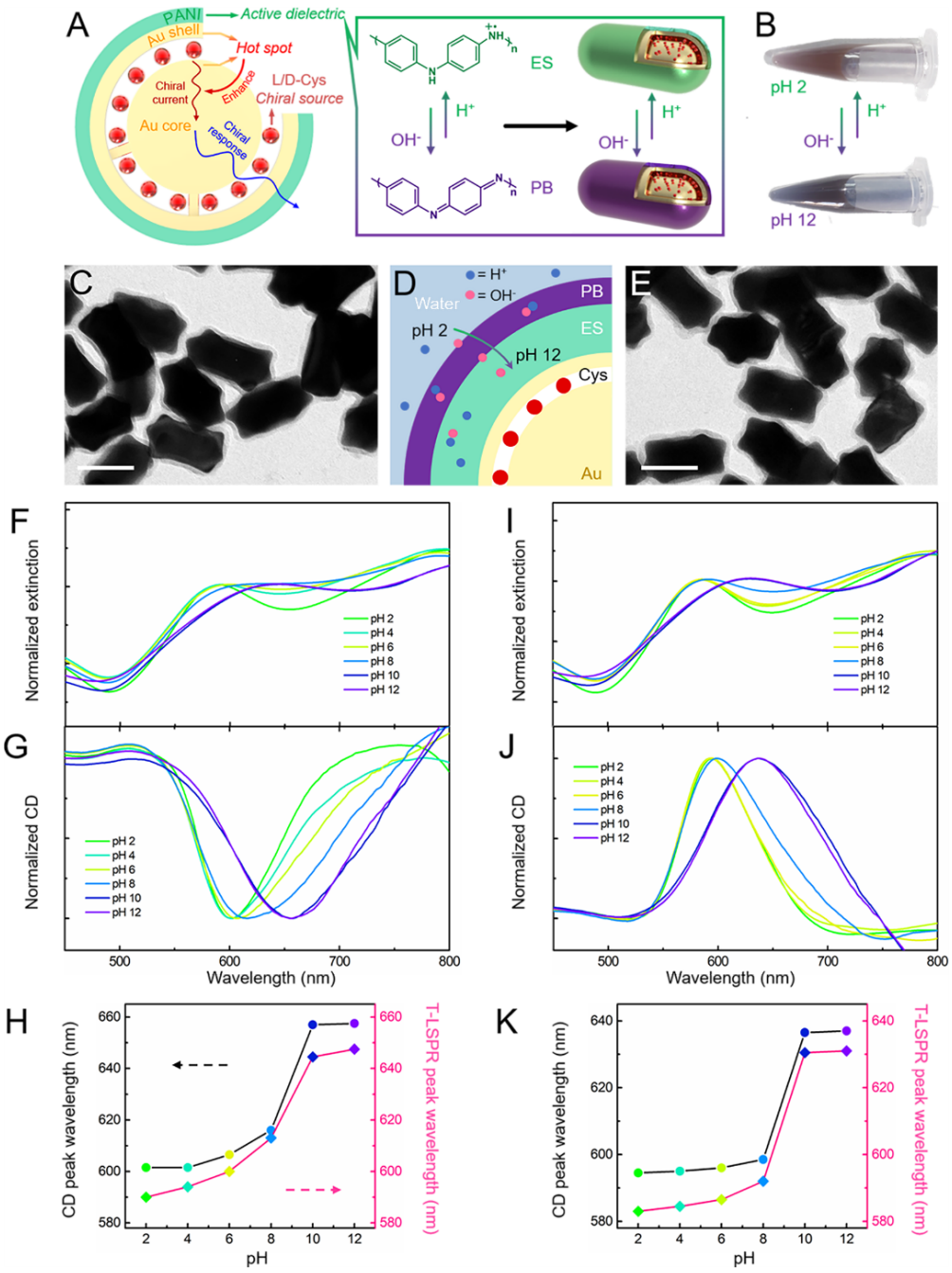

222

223 **Figure 3.** pH-modulated plasmonic and CD-switching behavior of c-CGS Au NRs (II)@PANI.
224 (A) Mechanism of the chiral signal amplification and dielectric environment switching by proton
225 doping and de-doping. (B) Digital image of L-c-CGS Au NRs (II)@PANI solutions at pH 2 and
226 pH 12. (C) TEM image of L-c-CGS Au NRs (II)@PANI. (D) Schematic representation of OH^-

entering the PANI microenvironment from solution at different pH values. (E) TEM image of D-c-CGS Au NRs (II)@PANI. (F) Normalized extinction spectra, (G) CD spectra of L-c-CGS Au NRs (II)@PANI and (H) their corresponding peak positions in response to different environmental pH values. (I) Normalized extinction spectra, (J) CD spectra of D-c-CGS Au NRs (II)@PANI and (K) their corresponding peak positions in response to different environmental pH values. The scale bars are 100 nm.

Electrical potential-responsive plasmonic and plasmon-induced chiral activities. Compared with pH modulation, manipulating the CD peak response with the assistance of electrical potential was definitely a more attractive strategy (Figure 4A).[35] To enable voltage manipulation and device fabrication, we employed a Langmuir-Blodgett (LB)-like technique in which a large monolayer film was formed by nanoparticle self-assembly at the water-oil interface and subsequently transferred onto the ITO surface (Figure 4B, C and S18). Here, the PANI layer also acted as a physical spacer to avoid strong coupling between particles, or between particles and the substrate, allowing the monolayer to display LSPR properties similar to that of discrete nanoparticles. In addition, the LB state exhibited no significant extinction in the visible and near-infrared regions (Figure S15C, D). Further, taking the L-c-CGS Au NRs (II)@PANI as an example, PANI was in the ES state under a higher voltage (0.4 V) and pH 2. The T-LSPR position of the monolayer was located near 592 nm, while the corresponding $CD_{T\text{-}LSPR}$ peak was located near 602 nm, which were slightly red-shifted compared to the corresponding peak positions of discrete nanoparticles. It should be noted that for some oriented solid samples, linear dichroism and linear birefringence are the main artifacts that may be observed during CD measurements.[53] To exclude the above effects, we confirmed the consistency of the chiral spectral information from different positions as well as the *g*-factor values (Figure S19). As the voltage was reduced to -0.3 V, the ES

state gradually transitioned to the LB state, and the T-LSPR and $CD_{T\text{-}LSPR}$ peaks both underwent the red-shifts of 12 nm and 14 nm to 604 nm and 616 nm, respectively (Figure 4D-F, S20A-C). The peak shapes of the D-c-CGS Au NRs (II)@PANI also showed similar red-shift trends (Figure 4G-I, S20D-F). These results supported our findings regarding the advantages offered by electrical potential as a stimulus source, such as achieving more accurate manipulation while avoiding sudden changes in signal output.

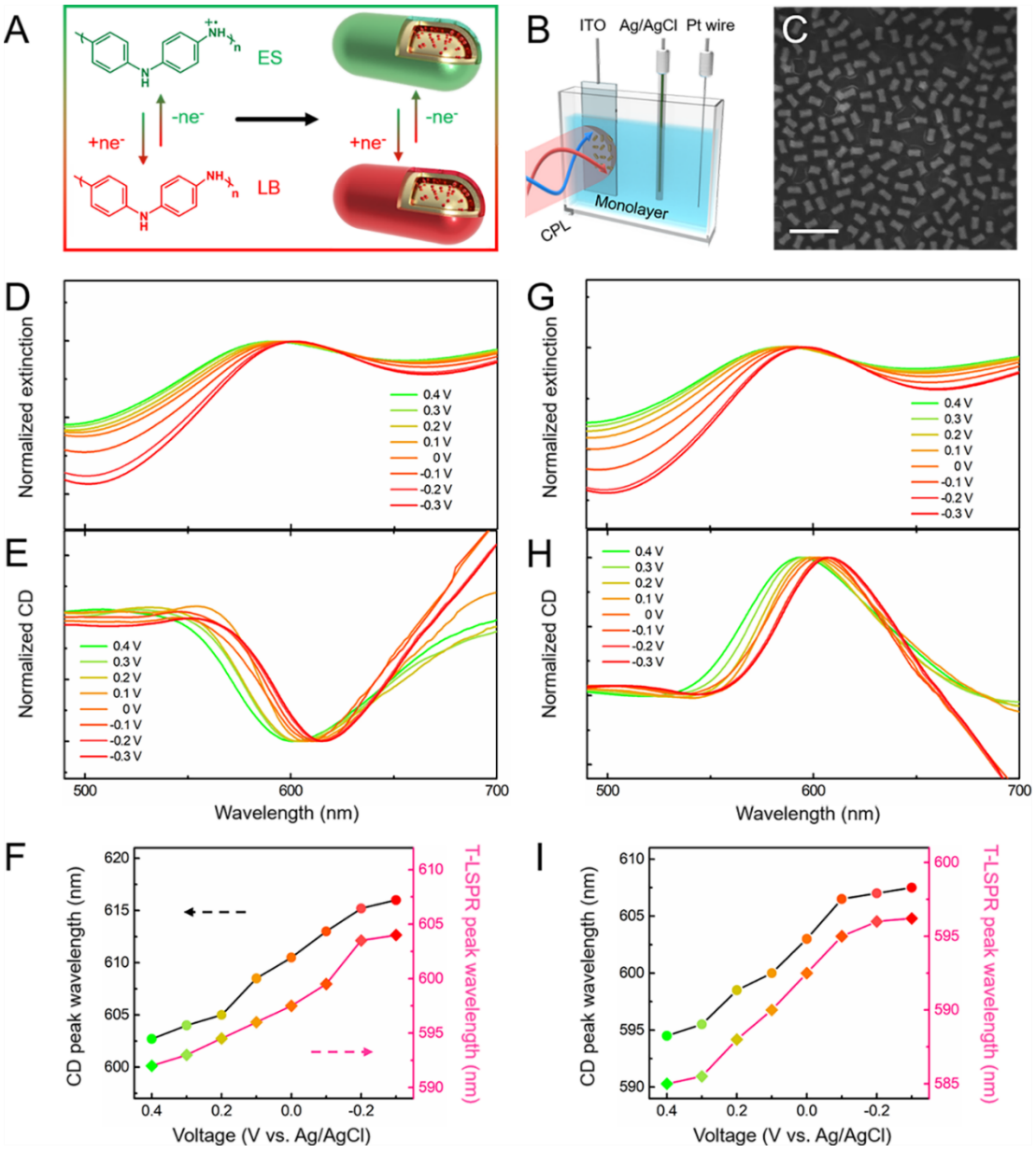

Figure 4. Electrical potential-modulated plasmonic and CD-switching behavior of a c-CGS Au NRs (II)@PANI monolayer film. (A) Mechanism of dielectric environment-switching by electrochemical redox. (B) Schematic illustration of the three-electrode electrochemical cell for the real-time measurement of the extinction and CD spectra of the c-CGS Au NRs (II)@PANI monolayers on an ITO substrate. (C) SEM image of large area L-c-CGS Au NRs (II)@PANI monolayer films loaded on an ITO surface. (D) Normalized extinction spectra and (E) CD spectra of L-c-CGS Au NRs (II)@PANI and (F) their corresponding peak positions in response to different voltages. (G) Normalized extinction spectra and (H) CD spectra of D-c-CGS Au NRs (II)@PANI and (I) their corresponding peak positions in response to different environmental pH values. The scale bar is 500 nm.

Stability, reversibility, and switching rate of LSPR and its chiroptical response. To further evaluate the LSPR and CD_{LSPR} dual response, the reversibility and stability of c-CGS Au NRs@PANI were investigated. Firstly, the L-c-CGS Au NRs (II)@PANI solution was switched in turn between pH 2 and pH 12. The shifts in the T-LSPR peak positions and the corresponding $CD_{T\text{-}LSPR}$ peak positions presented good reversibility during the five cycles (Figure 5A). The electrical potential group also showed stable performance over the same cycles (Figure 5B). The extinction intensity, chiral response and electrochemical activity curves did not degrade significantly before or after 100 scan cycles, indicating the good reproducibility of the ES and LB states based on electrical potential switching (Figure 5C-E, S21). Finally, as it was not easy to record instantaneous extinction spectra as in other reports,[36] we measured the falling current stabilization time to reflect the switching rates of the monolayer by using the amperometric i-t method at a fixed voltage, which is approximately 500 ms (Figure 5F).[54] The larger signal shifts from pH modulation and the small range of precise responses from electrical potential modulation

reflect the complementary advantages of this material in terms of suitability to different optical scenarios with excellent reversibility and stability.

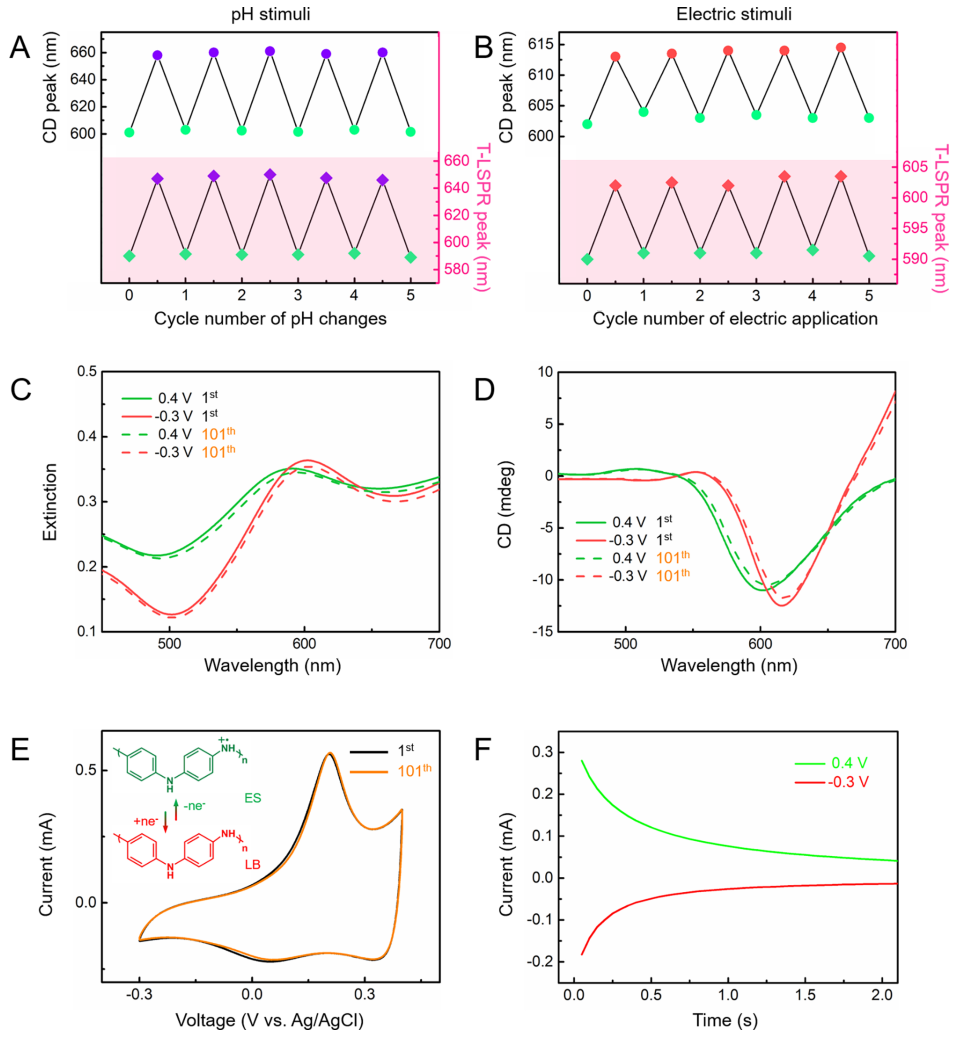

Figure 5. Electrochemical response performance. (A) Peak positions corresponding to extinction (squares) and CD (circles) of L-c-CGS Au NRs (II)@PANI at pH 2 (green) or pH 12 (purple) during five cycles. (B) Peak positions corresponding to extinction (squares) and CD (circles) of L-c-CGS Au NRs (II)@PANI monolayers at 0.4 V (green) or -0.3 V (red) during five cycles. (C) Extinction spectra of L-c-CGS Au NRs (II)@PANI monolayers at 0.4 V (green) and -0.3 V(red) before and after 100 scans. (D) CD spectra of L-c-CGS Au NRs (II)@PANI monolayers at 0.4 V

(green) and -0.3 V(red) before and after 100 scans. (E) Cyclic voltammograms of L-c-CGS Au NRs (II)@PANI monolayers before and after 100 scans. (F) Switching time of L-c-CGS Au NRs (II)@PANI monolayers at fixed voltages of 0.4 V (green) and -0.3 V (red).

Conclusion

In summary, we demonstrated a simple and robust bottom-up wet chemical approach to the synthesis of discrete gold nanostructures with dynamically tunable electrochemical plasmonic chiroptical activities. Uniquely, this study focused on the induction of a well-defined $CD_{T\text{-}LSPR}$ from an inconspicuous T-LSPR in the extinction spectra that provides the potential for chiroptical activity tuning. With external stimuli such as pH or electric potential, the $CD_{T\text{-}LSPR}$ all responded with similar peak wavelength shifts as the T-LSPR. Meanwhile, the c-CGS Au NRs (II)@PANI showed excellent stability and reversibility, the ability to switch optical features in real-time, as well as flexible designability and processability. The above properties indicate that a similarly well-defined discrete active plasmonic structure could be a strong candidate for the fabrication of novel optical devices, such as optical switches, transducers and filters.

Experimental Section

Materials. Chloroauric acid ($HAuCl_4 \cdot 3H_2O$, 99.9%) and D-cysteine (>99.0%) were purchased from Sigma-Aldrich. Cetrimonium bromide (CTAB, >99.0%), hexadecyltrimethylammonium chloride (CTAC, ≥95.0%) and L-cysteine (>98.0%) were purchased from TCI (Shanghai). Sodium borohydride ($NaBH_4$, 99.0%), ascorbic acid (AA, 99.7%), silver nitrate ($AgNO_3$, >99.0%), hydrochloric acid (HCl, 37 wt% in water) and *n*-hexane (GR)

were obtained from Sinopharm Chemical Reagent Co., Ltd. (Shanghai). Sodium dodecyl sulfate (SDS, ACS, ≥99.0%), aniline (ACS, ≥99.0%), ammonium persulfate (AR, ≥98%), sodium hypochlorite solution (NaClO, available chlorine 6-15%) and anhydrous ethanol were purchased from Aladdin.

Characterization. UV−vis and CD spectra were recorded by a TU-1810 spectrophotometer (Purkinje General Instrument Co., Ltd.) and Jasco J-1700-150 spectropolarimeter, respectively. Field-emission scanning electron microscopy (FE-SEM) observation was carried out using an S-4800 instrument (Hitachi) at an acceleration voltage of 8 kV. Transmission electron microscopy (TEM) was performed on a JEM-2100F electron microscope operating at 200 kV. Electrochemical measurements were performed on a CHI 760E electrochemical workstation (Chenhua Instrument Company, Shanghai, China).

Synthesis of Au NSs and Au NRs. CTAC-coated gold nanospheres (Au NSs) were prepared according to the seed-mediated growth method with minor modifications.[55] Firstly, Au seeds were prepared by injecting fresh ice-cold $NaBH_4$ aqueous solution (0.2 mL, 20 mM) into a mixture of $HAuCl_4$ (0.1 mL, 25 mM) and CTAC (5 mL, 0.1 M) solution with vigorous stirring for 3 min, and the mixture was let stand undisturbed for 30 min to allow the excess $NaBH_4$ to age out. The resulting Au seed solution (90 μL) was injected into a mixture of AA (40 μL, 0.1 M) and CTAC (10 mL, 25 mM), and then stirred for 5 min. Next, $HAuCl_4$ solution (100 μL, 25 mM) was injected, stirred vigorously for 1 min, and incubated for 20 min to obtain the bigger Au seeds (diameter: 10 nm). Further growth was achieved by adding $HAuCl_4$ solution (200 μL, 25 mM) to a mixture of AA (80 μL, 0.1 M), CTAC (20 mL, 25 mM) and Au seeds (10 nm, 50 μL). After stirring vigorously for 30 s, the solution was let stand undisturbed for at least 1.5 h. Subsequently, a diluted NaClO solution (available chlorine 1-2.5%, 20 μL) was injected to neutralize the excess AA, and the first

etching was completed. After rapid stirring for 5 min, $HAuCl_4$ (10 μL, 25 mM) was added while stirring for 30 s, and the mixture was then incubated for 1 h to complete the second etching. Finally, homogeneous CTAC-coated Au NSs (diameter: 50 nm) were obtained after centrifugation (3405 ×*g*).

CTAC-coated Au NRs were prepared according to the previously reported seed-mediated method.[56] First, the seed solution was prepared by rapid injection of fresh ice-cold $NaBH_4$ aqueous solution (0.6 mL, 10 mM) into a mixture of $HAuCl_4$ (0.1 mL, 25 mM) and CTAB (9.9 mL, 0.1 M) with vigorous stirring for 2 min. The color of the seed solution changed from yellow to brown. The seed solution was left undisturbed for at least 30 min before use. The growth solution was prepared by mixing CTAB solution (200 mL, 0.1 M) with $AgNO_3$ solution (6 mL, 10 mM) and letting it stand undisturbed at 30 °C for 15 min. $HAuCl_4$ solution (4 mL, 25 mM) was then added and the mixture stirred (700 rpm) for 30 min. Subsequently, HCl (0.35 mL, 12.1 M) was added and the mixture stirred (400 rpm) for 15 min. AA solution (1.6 mL, 0.1 M) was then added and the mixture stirred vigorously (1200 rpm) for 30 s, followed by the injection of 20 μL of the above seed solution with vigorous stirring (1500 rpm) for 30 s. The mixed solution was then left undisturbed at 30 °C for 12 h to allow Au NRs growth. Finally, the resulting Au NRs were centrifuged (4448 ×*g*, 10 min) and redispersed in CTAC solution (100 mL, 80 mM) twice for further use. A 8*20-mm shuttle rotor was used.

Synthesis of c-CGS Au NRs and Au NSs. Chiral gold nanostructures were prepared by the previously reported with minor modifications.[40] CTAC-coated Au NRs or Au NSs (250 μL) were injected into a mixture of $HAuCl_4$ (25 μL, 1 mM), CTAC (1 mL, 40 mM), AA (20 μL, 0.1 M) and L- or D-Cys (180 μL), shaken gently for 10 s and incubated for 1 h at room temperature. Subsequently, $HAuCl_4$ (25 μL, 1 mM) was injected, shaken gently for 10 s, and incubated for 2 h.

The final concentration of L- or D-Cys was maintained at 5 nM, 50 nM and 500 nM, corresponding to products including c-CGS Au NRs (I), c-CGS Au NRs (II) and c-CGS Au NRs (III), respectively. After centrifugation (3405 ×*g*, 10 min) and redispersal in CTAC solution (1.5 mL, 5 mM) to remove excess Cys, c-CGS Au NRs or c-CGS Au NSs were obtained. To further confirm the main chiral signal came from the encapsulated Cys molecules, c-CGS Au NRs were treated using $NaBH_4$ solution (40 mM) and re-dissolved in CTAC solution (40 mM) used for CD measurements, since $NaBH_4$ could remove any thiols from the gold surface.[57]

Synthesis of c-CGS Au NRs@PANI. The coating of Au NRs or Au NSs with PANI was realized by surfactant-assisted chemical oxidative polymerization.[32] The as-synthesized c-CGS Au NRs (II) (1.5 mL) were centrifuged, and the precipitate was redispersed in a mixture of aniline (25 μL, 44 mM) and SDS (37.5 μL, 40 mM) and shaken vigorously for 1 min. Subsequently, the above solution was mixed with an acidic $(NH_4)_2S_2O_8$ solution (200 μL, 2 mM in 10 mM HCl) and further shaken for 1 min. Finally, it was let stand undisturbed overnight to obtain the c-CGS Au NRs@PANI. To remove free PANI after the polymerization process, the supernatant was removed by centrifugation (2936 ×*g*, 10 min) and the precipitate was redispersed in SDS solution (1 mL, 5 mM). The PANI coating of the Au NSs followed the same procedure as that for the Au NRs.

Fabrication and transfer of c-CGS Au NRs@PANI monolayers. The c-CGS Au NRs@PANI monolayer film was prepared based on our previous work [33, 58] with some minor modifications. Briefly, c-CGS Au NRs@PANI solution (7 mL) and deionized water (3 mL) were added to a clean glass culture dish (diameter: 6 cm) and mixed well, then hexane solution (10 mL) was slowly added to the surface of the above solution to form an immiscible water-oil interface. The anhydrous ethanol (10 mL) was injected into the aqueous phase solution at a uniform rate (0.8 mL/min) via a mechanical syringe pump. This strategy enabled the nanoparticles in the aqueous

phase to gradually transfer to the water-oil interface and self-assemble into a monolayer film. After the injection, the culture dish was covered with a glass sheet to control the slow evaporation of the hexane until the film was completely exposed to the water-air interface. Subsequently, an indium tin oxide (ITO) electrode was touched to the monolayer film surface at a specific inclination angle, so that the film was smoothly transferred to the ITO surface by capillary forces. After immersion in water overnight to remove excess SDS, the film was then transferred to an HCl solution (0.1 M) for 1 h to ensure that the PANI was completely converted to an emeraldine salt (ES) state.

Dual response of c-CGS Au NRs@PANI for plasmonic and chiral spectroscopic properties. The pH stimulation of LSPR and the chiral spectroscopic properties of c-CGS Au NRs@PANI were realized with HCl (0.1 M) and NaOH (0.1 M). To ensure the complete doping/de-doping of the internal protons of PANI, oscillation for 30 s was necessary before spectroscopic measurements. With regard to potential stimulation, we used a classical three-electrode system consisting of an ITO-loaded c-CGS Au NRs@PANI monolayer film as the working electrode, a platinum wire electrode as the counter electrode, and an Ag/AgCl (3 M KCl) electrode as the reference electrode. In order to achieve the gentle transitions between ES, LB and PB states and to avoid electrochemical degradation of the PANI layer, damage to the ITO substrate and potential hydrogen evolution reactions,[36] the HCl solution (0.01 M) with NaCl (0.5 M) was used as the electrolyte, and the voltage window was limited to 0.4 V to -0.3 V. UV-vis and CD spectra were recorded simultaneously after pH and electric potential stimulation. Cyclic voltammetric measurements were performed at a scan rate of 0.1 V/s. To better compare the LSPR shift responses, all normalized spectra as well as the CD spectra were converted from transverse LSPR (T-LSPR) intensity to a value of 1.

Calculation of the *g*-factor. The asymmetry factor of the polarization rotation, also known as the *g*-factor, is a concentration-independent parameter. It is calculated as the ratio of the different absorbances of a substance between LCP light and RCP light to the total absorbance using the following equation:[59]

$$g\text{-factor}=\frac{A_{LCP}-A_{RCP}}{A_{LCP}+A_{RCP}}=\frac{\Delta A}{A_{total}}\approx\frac{CD(mdeg)}{32980\cdot Abs}$$

Associated Content

Supporting Information

The Supporting Information is available free of charge at

TEM images, extinction and CD spectra of Au NRs; chemical structures, extinction and CD spectra of L/D Cys; growth mechanisms for c-CGS Au NRs; TEM images of c-CGS Au NRs (II); CD spectra of Au NRs@L-Cys and L-c-CGS Au NRs (II); *g*-factor diagrams of c-CGS Au NRs (I) and (II), (III); TEM images of Au NSs, L-c-CGS Au NSs and D-c-CGS Au NSs; CD spectra of Au NSs@L-Cys and c-CGS Au NSs (II); *g*-factor diagrams of L-c-CGS Au NRs (II), L-c-CGS Au NRs (II)@PANI, L-c-CGS Au NRs and L-c-CGS Au NRs@PANI; TEM images of c-CGS Au NSs@PANI; normalized extinction spectra of Au NSs, c-CGS Au NSs and c-CGS Au NSs@PANI; digital images and normalized extinction spectra of pure PANI solution in the ES and PB states; normalized extinction spectra of c-CGS Au NSs@$PANI_{(ES)}$, c-CGS Au NSs@$PANI_{(PB)}$ and c-CGS Au NSs@$PANI_{(LB)}$; extinction spectra of L-c-CGS Au NRs (II) with different PANI layer thicknesses;

digital images of c-CGS Au NRs (II)@PANI large area monolayers; and electrochemical cycling test of D-c-CGS Au NRs (II)@PANI.

Author information

Corresponding Authors

Hideyuki Mitomo - Research Institute for Electronic Science, Hokkaido University, Kita 21, Nishi 10, Kita-Ku, Sapporo, 001-0021, Japan; Email: mitomo@es.hokudai.ac.jp

Zhiyong Guo - State Key Laboratory for Managing Biotic and Chemical Threats to the Quality and Safety of Agro-products, School of Material Science and Chemical Engineering, Ningbo University, Ningbo 315211, PR China; Email: guozhiyong@nbu.edu.cn

Kuniharu Ijiro - Research Institute for Electronic Science, Hokkaido University, Kita 21, Nishi 10, Kita-Ku, Sapporo, 001-0021, Japan; Email: ijiro@es.hokudai.ac.jp

Author

Han Lin - Graduate School of Life Science, Hokkaido University, Kita 10, Nishi 8, Kita-Ku, Sapporo, 060-0810, Japan

Yusuke Yonamine - Research Institute for Electronic Science, Hokkaido University, Kita 21, Nishi 10, Kita-Ku, Sapporo, 001-0021, Japan

Author Contributions

The manuscript was written through contributions from all authors. All authors have approved the final version of the manuscript.

Acknowledgements

H. M. appreciates support from the Creative Research Institute (CRIS) in Hokkaido University. K. I. acknowledges support from the Photoexcitonix Project and the Young Investigator Promotion Project in Hokkaido University. Z. G. gratefully acknowledges the National Natural Science Foundation of China (Grant No. 42076193, 81773483). This work was supported in part by the "Dynamic Alliance for Open Innovation Bridging Human, Environment and Materials" from the Ministry of Education, Culture, Sports, Science and Technology of Japan (MEXT).

Notes

The authors declare no competing financial interests.

References

1. Kelvin, L. W. T. *Baltimore Lectures on Molecular Dynamics and the Wave Theory of Light*. C. J. Clay and Sons, London, **1904;** pp 436.

2. Davis, W. B.; Svec, W. A.; Ratner, M. A.; Wasielewski, M. R. Molecular-wire behaviour in p -phenylenevinylene oligomers. *Nature* **1998,** *396*, 60-63.

3. Berova, N.; Nakanishi, K.; Woody, R. *Circular Dichroism: Principles and Applications*. 2nd ed.; Wiley-VCH: New York, **2000;** pp 877.

4. Govorov, A. O.; Fan, Z.; Hernandez, P.; Slocik, J. M.; Naik, R. R. Theory of Circular Dichroism of Nanomaterials Comprising Chiral Molecules and Nanocrystals: Plasmon Enhancement, Dipole Interactions, and Dielectric Effects. *Nano Lett*. **2010,** *10*, 1374-1382.

5. Nesterov, M. L.; Yin, X.; Schäferling, M.; Giessen, H.; Weiss, T. The Role of Plasmon-Generated Near Fields for Enhanced Circular Dichroism Spectroscopy. *ACS Photonics* **2016,** *3*, 578-583.

6. Chulhai, D. V.; Jensen, L. Plasmonic Circular Dichroism of 310- and α-Helix Using a Discrete Interaction Model/Quantum Mechanics Method. *J. Phys. Chem. A* **2014,** *119*, 5218-5223.

7. Ben-Moshe, A.; Maoz, B. M.; Govorov, A. O.; Markovich, G. Chirality and Chiroptical Effects in Inorganic Nanocrystal Systems with Plasmon and Exciton Resonances. *Chem. Soc. Rev.* **2013,** *42*, 7028-7041.

8. Ma, W.; Kuang, H.; Xu, L.; Ding, L.; Xu, C.; Wang, L.; Kotov, N. A. Attomolar DNA Detection with Chiral Nanorod Assemblies. *Nat. Commun.* **2013,** *4*, 2689.

9. Wu, X.; Xu, L.; Liu, L.; Ma, W.; Yin, H.; Kuang, H.; Wang, L.; Xu, C.; Kotov, N. A. Unexpected Chirality of Nanoparticle Dimers and Ultrasensitive Chiroplasmonic Bioanalysis. *J. Am. Chem. Soc.* **2013,** *135*, 18629-18636.

10. Zheng, G.; He, J.; Kumar, V.; Wang, S.; Pastoriza-Santos, I.; Pérez-Juste, J.; Liz-Marzán, L. M.; Wong, K.-Y. Discrete Metal Nanoparticles with Plasmonic Chirality. *Chem. Soc. Rev.* **2021,** *50*, 3738-3754.

11. Urban, M. J.; Shen, C.; Kong, X.-T.; Zhu, C.; Govorov, A. O.; Wang, Q.; Hentschel, M.; Liu, N. Chiral Plasmonic Nanostructures Enabled by Bottom-Up Approaches. *Annu. Rev. Phys. Chem.* **2019,** *70*, 275-299.

12. Ma, W.; Xu, L.; de Moura, A. F.; Wu, X.; Kuang, H.; Xu, C.; Kotov, N. A. Chiral Inorganic Nanostructures. *Chem. Rev.* **2017,** *117*, 8041-8093.

13. Im, S. W.; Ahn, H. Y.; Kim, R. M.; Cho, N. H.; Kim, H.; Lim, Y. C.; Lee, H. E.; Nam, K. T. Chiral Surface and Geometry of Metal Nanocrystals. *Adv. Mater.* **2019,** *32*, 1905758.

14. Severoni, E.; Maniappan, S.; Liz-Marzán, L. M.; Kumar, J.; García de Abajo, F. J.; Galantini, L. Plasmon-Enhanced Optical Chirality through Hotspot Formation in Surfactant-Directed Self-Assembly of Gold Nanorods. *ACS Nano* **2020,** *14*, 16712-16722.

15. Nguyen, L.; Dass, M.; Ober, M. F.; Besteiro, L. V.; Wang, Z. M.; Nickel, B.; Govorov, A. O.; Liedl, T.; Heuer-Jungemann, A. Chiral Assembly of Gold–Silver Core–Shell Plasmonic Nanorods on DNA Origami with Strong Optical Activity. *ACS Nano* **2020,** *14*, 7454-7461.

16. Wu, Z.; Zheng, Y. Moiré Chiral Metamaterials. *Adv. Opt. Mater.* **2017,** *5*, 1700034.

17. Wang, X.; Tang, Z. Circular Dichroism Studies on Plasmonic Nanostructures. *Small* **2017,** *13*, 1601115.

18. Wu, Z.; Chen, X.; Wang, M.; Dong, J.; Zheng, Y. High-Performance Ultrathin Active Chiral Metamaterials. *ACS Nano* **2018,** *12*, 5030-5041.

19. Zhou, C.; Duan, X.; Liu, N. DNA-Nanotechnology-Enabled Chiral Plasmonics: From Static to Dynamic. *Acc. Chem. Res.* **2017,** *50*, 2906-2914.

20. Man, T.; Ji, W.; Liu, X.; Zhang, C.; Li, L.; Pei, H.; Fan, C. Chiral Metamolecules with Active Plasmonic Transition. *ACS Nano* **2019,** *13*, 4826-4833.

21. Lan, X.; Liu, T.; Wang, Z.; Govorov, A. O.; Yan, H.; Liu, Y. DNA-Guided Plasmonic Helix with Switchable Chirality. *J. Am. Chem. Soc.* **2018,** *140*, 11763-11770.

22. Nguyen, M.-K.; Kuzyk, A. Reconfigurable Chiral Plasmonics beyond Single Chiral Centers. *ACS Nano* **2019,** *13*, 13615-13619.

23. Querejeta-Fernández, A.; Chauve, G.; Methot, M.; Bouchard, J.; Kumacheva, E. Chiral Plasmonic Films Formed by Gold Nanorods and Cellulose Nanocrystals. *J. Am. Chem. Soc.* **2014,** *136*, 4788-4793.

24. Querejeta-Fernández, A.; Kopera, B.; Prado, K. S.; Klinkova, A.; Methot, M.; Chauve, G.; Bouchard, J.; Helmy, A. S.; Kumacheva, E. Circular Dichroism of Chiral Nematic Films of Cellulose Nanocrystals Loaded with Plasmonic Nanoparticles. *ACS Nano* **2015,** *9*, 10377-10385.

25. Schreiber, R.; Luong, N.; Fan, Z.; Kuzyk, A.; Nickels, P. C.; Zhang, T.; Smith, D. M.; Yurke, B.; Kuang, W.; Govorov, A. O.; Liedl, T. Chiral Plasmonic DNA Nanostructures with Switchable Circular Dichroism. *Nat. Commun.* **2013,** *4*, 2948.

26. Probst, P. T.; Mayer, M.; Gupta, V.; Steiner, A. M.; Zhou, Z.; Auernhammer, G. K.; König, T. A. F.; Fery, A. Mechano-Tunable Chiral Metasurfaces via Colloidal Assembly. *Nat. Mater.* **2021,** *20*, 1024-1028.

27. Nakamura, S.; Mitomo, H.; Yonamine, Y.; Ijiro, K. Salt-Triggered Active Plasmonic Systems Based on the Assembly/Disassembly of Gold Nanorods in a DNA Brush Layer on a Solid Substrate. *Chem. Lett.* **2020,** *49*, 749-752.

28. Jiang, N.; Zhuo, X.; Wang, J. Active Plasmonics: Principles, Structures, and Applications. *Chem. Rev.* **2017,** *118*, 3054-3099.

29. Liu, B.; Lu, X.; Qiao, Z.; Song, L.; Cheng, Q.; Zhang, J.; Zhang, A.; Huang, Y.; Chen, T. pH and Temperature Dual-Responsive Plasmonic Switches of Gold Nanoparticle Monolayer Film for Multiple Anticounterfeiting. *Langmuir* **2018,** *34*, 13047-13056.

30. Iida, R.; Mitomo, H.; Niikura, K.; Matsuo, Y.; Ijiro, K. Two-Step Assembly of Thermoresponsive Gold Nanorods Coated with a Single Kind of Ligand. *Small* **2018,** *14*, 1704230.

31. Baker, C. O.; Huang, X.; Nelson, W.; Kaner, R. B. Polyaniline Nanofibers: Broadening Applications for Conducting Polymers. *Chem. Soc. Rev.* **2017,** *46*, 1510-1525.

32. Jiang, N.; Shao, L.; Wang, J. (Gold Nanorod Core)/(Polyaniline Shell) Plasmonic Switches with Large Plasmon Shifts and Modulation Depths. *Adv. Mater.* **2014,** *26*, 3282-3289.

33. Lin, H.; Song, L.; Huang, Y.; Cheng, Q.; Yang, Y.; Guo, Z.; Su, F.; Chen, T. Macroscopic Au@PANI Core/Shell Nanoparticle Superlattice Monolayer Film with Dual-Responsive Plasmonic Switches. *ACS Appl. Mater. Interfaces* **2020,** *12*, 11296-11304.

34. Jeon, J.-W.; Zhou, J.; Geldmeier, J. A.; Ponder, J. F.; Mahmoud, M. A.; El-Sayed, M.; Reynolds, J. R.; Tsukruk, V. V. Dual-Responsive Reversible Plasmonic Behavior of Core–Shell Nanostructures with pH-Sensitive and Electroactive Polymer Shells. *Chem. Mater.* **2016,** *28*, 7551-7563.

35. Jeon, J.-W.; Ledin, P. A.; Geldmeier, J. A.; Ponder, J. F.; Mahmoud, M. A.; El-Sayed, M.; Reynolds, J. R.; Tsukruk, V. V. Electrically Controlled Plasmonic Behavior of Gold Nanocube@Polyaniline Nanostructures: Transparent Plasmonic Aggregates. *Chem. Mater.* **2016,** *28*, 2868-2881.

36. Lu, W.; Jiang, N.; Wang, J. Active Electrochemical Plasmonic Switching on Polyaniline-Coated Gold Nanocrystals. *Adv. Mater.* **2017,** *29*, 1604862.

37. Hentschel, M.; Schäferling, M.; Duan, X.; Giessen, H.; Liu, N. Chiral Plasmonics. *Sci. Adv.* **2021,** *7*, e1602735.

38. Wang, G.; Liu, Y.; Gao, C.; Guo, L.; Chi, M.; Ijiro, K.; Maeda, M.; Yin, Y. Island Growth in the Seed-Mediated Overgrowth of Monometallic Colloidal Nanostructures. *Chem* **2017,** *3*, 678-690.

39. Kim, J. M.; Lee, C.; Lee, Y.; Lee, J.; Park, S. J.; Park, S.; Nam, J. M. Synthesis, Assembly, Optical Properties, and Sensing Applications of Plasmonic Gap Nanostructures. *Adv. Mater.* **2021,** *33*, 2006966.

40. Zheng, G.; Bao, Z.; Pérez-Juste, J.; Du, R.; Liu, W.; Dai, J.; Zhang, W.; Lee, L. Y. S.; Wong, K.-Y. Tuning the Morphology and Chiroptical Properties of Discrete Gold Nanorods with Amino Acids. *Angew. Chem., Int. Ed.* **2018,** *57*, 16452-16457.

41. Behar-Levy, H.; Neumann, O.; Naaman, R.; Avnir, D. Chirality Induction in Bulk Gold and Silver. *Adv. Mater.* **2008,** *19*, 1207-1211.

42. Hou, S.; Yan, J.; Hu, Z.; Wu, X. Enhancing the Plasmonic Circular Dichroism by Entrapping Chiral Molecules at the Core-Shell Interface of Rod-Shaped Au@Ag Nanocrystals. *Chem. Commun.* **2016**, *52*, 2059-2062.

43. Wu, X.; Xu, L.; Ma, W.; Liu, L.; Kuang, H.; Yan, W.; Wang, L.; Xu, C. Gold Core-DNA-Silver Shell Nanoparticles with Intense Plasmonic Chiroptical Activities. *Adv. Funct. Mater.* **2015,** *25*, 850-854.

44. Wang, Y.; He, W.; Li, C.; Xia, C.; Yan, Y.; Li, C.; Huang, C. Chirality Transfer of Cysteine to the Plasmonic Resonance Region through Silver Coating of Gold Nanobipyramids. *Chem. Commun.* **2021,** *57*, 3211-3214.

45. He, J.; Wang, Y.; Feng, Y.; Qi, X.; Zeng, Z.; Liu, Q.; Teo, W. S.; Gan, C. L.; Zhang, H.; Chen, H. Forest of Gold Nanowires: A New Type of Nanocrystal Growth. *ACS Nano* **2013,** *7*, 2733-2740.

566 46. Govorov, A. O. Plasmon-Induced Circular Dichroism of a Chiral Molecule in the Vicinity of
567 Metal Nanocrystals. Application to Various Geometries. *J. Phys. Chem. C* **2011,** *115*, 7914-
568 7923.

569 47. Govorov, A. O.; Z. Fan. Theory of Chiral Plasmonic Nanostructures Comprising Metal
570 Nanocrystals and Chiral Molecular Media. *ChemPhysChem* **2012,** *13*, 2551-2560.

571 48. González-Rubio, G.; Mosquera, J.; Kumar, V.; Pedrazo-Tardajos, A.; Llombart, P.; Solís, D.
572 M.; Lobato, I.; Noya, E. G.; Guerrero-Martínez, A.; Taboada, J. M.; Obelleiro, F.; MacDowell,
573 L. G.; Bals, S.; Liz-Marzán, L. M. Micelle-Directed Chiral Seeded Growth on Anisotropic Gold
574 Nanocrystals. *Science* **2020,** *368*, 1472-1477.

575 49. Lee, H.-E.; Ahn, H.-Y.; Mun, J.; Lee, Y. Y.; Kim, M.; Cho, N. H.; Chang, K.; Kim, W. S.;
576 Rho, J.; Nam, K. T. Amino-Acid- and Peptide-Directed Synthesis of Chiral Plasmonic Gold
577 Nanoparticles. *Nature* **2018,** *556*, 360-365.

578 50. Kong, X. T.; Besteiro, L. V.; Wang, Z.; Govorov, A. O. Plasmonic Chirality and Circular
579 Dichroism in Bioassembled and Nonbiological Systems: Theoretical Background and Recent
580 Progress. *Adv. Mater.* **2018,** *32*, 1801790.

581 51. Lu, Y.; Lam, S. H.; Lu, W.; Shao. L.; Chow, T. H.; Wang, J. All-State Switching of the Mie
582 Resonance of Conductive Polyaniline Nanospheres. *Nano Lett.* **2022,** *22*, 1406-1414.

583 52. Chen, H.; Shao, L.; Li, Q.; Wang, J. Gold Nanorods and Their Plasmonic Properties. *Chem.*
584 *Soc. Rev.* **2013,** *42*, 2679-2724.

585 53. Merten, C.; Kowalik, T.; Hartwig, A. Vibrational Circular Dichroism Spectroscopy of Solid
586 Polymer Films: Effects of Sample Orientation. *Appl. Spectrosc.* **2008,** *62*, 901-905.

587 54. Kaissner, R.; Li, J.; Lu, W.; Li, X.; Neubrech, F.; Wang, J.; Liu, N. Electrochemically
588 Controlled Metasurfaces with High-contrast Switching at Visible Frequencies. *Sci. Adv.* **2021,** *7*,
589 eabd9450.

590 55. Hanske, C.; González-Rubio, G.; Hamon, C.; Formentín, P.; Modin, E.; Chuvilin, A.;
591 Guerrero-Martínez, A.; Marsal, L. F.; Liz-Marzán, L. M. Large-Scale Plasmonic Pyramidal
592 Supercrystals via Templated Self-Assembly of Monodisperse Gold Nanospheres. *J. Phys. Chem.*
593 *C* **2017,** *121*, 10899-10906.

594 56. Ni, W.; Kou, X.; Yang, Z.; Wang, J. Tailoring Longitudinal Surface Plasmon Wavelengths,
595 Scattering and Absorption Cross Sections of Gold Nanorods. *ACS Nano* **2008,** *2*, 677-686.

596 57. Ansar, S. M.; Ameer, F. S.; Hu, W.; Zou, S.; Pittman, C. U.; Zhang, D. Removal of
597 Molecular Adsorbates on Gold Nanoparticles Using Sodium Borohydride in Water. *Nano Lett.*
598 **2013,** *13*, 1226-1229.

599 58. Lu, X.; Huang, Y.; Liu, B.; Zhang, L.; Song, L.; Zhang, J.; Zhang, A.; Chen, T. Light-
600 Controlled Shrinkage of Large-Area Gold Nanoparticle Monolayer Film for Tunable SERS
601 Activity. *Chem. Mater.* **2018,** *30*, 1989-1997.

59. Yan, J.; Feng, W.; Kim, J.-Y.; Lu, J.; Kumar, P.; Mu, Z.; Wu, X.; Mao, X.; Kotov, N. A. Self-Assembly of Chiral Nanoparticles into Semiconductor Helices with Tunable near-Infrared Optical Activity. *Chem. Mater.* **2019,** *32*, 476-488.

Table of Contents